ACS Catalysis

pubs.acs.org/acscatalysis Letter

Ionomer Side Chains Modulate Interfacial Microenvironments for Selective CO_2 Electrolysis

Jihyun Park,[⊥] Younghyun Chae,[⊥] Chanwoo Lee, Gyeongjin Kwon, Woong Hee Lee, Hyo Sang Jeon, Jinhan Cho, Da Hye Won,* and Jai Hyun Koh*

Cite This: *ACS Catal.* 2025, 15, 12222−12230 Read Online

ACCESS | Metrics & More | Article Recommendations | Supporting Information

ABSTRACT: This study investigates how the molecular structure of imidazolium ionomers with linear alkyl side chains (C_nH_{2n+1} where n = 1, 4, 10, 16) modulates interfacial microenvironments in the Ag-catalyzed CO_2 reduction reaction (CO_2RR). Variations in side chain length and molecular weight establish structure−performance relationships that link hydrophobicity and ion transport to activity and selectivity. Longer side chains suppress hydrogen evolution and enhance the CO_2RR, with the n-hexadecyl ionomer achieving the highest Faradaic efficiency for the CO_2RR of 90.1% in a two-compartment cell. Incorporation of this ionomer in a cation-exchange membrane-based membrane electrode assembly achieves selective CO production with a partial current density exceeding 100 mA cm^{-2}, outperforming a commercial benchmark. Controlled studies under lean and acidic electrolytes reveal that the ionomer maintains local alkaline environments by restricting the interfacial water and proton transport. These findings provide molecular-level insights into ionomer function and design principles for selective CO_2RR in practical electrolyzers.

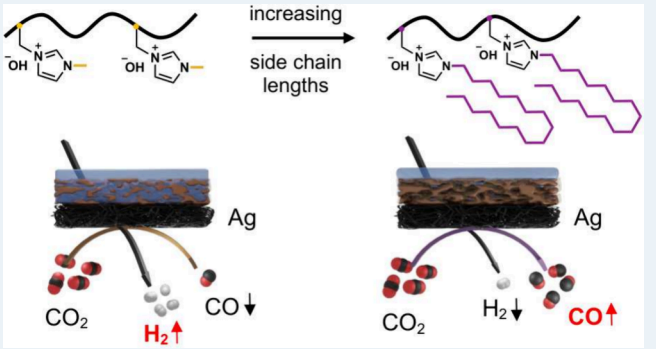

KEYWORDS: *CO_2 reduction, Ag catalyst, ionomer, microenvironment, MEA*

1. INTRODUCTION

Ion-conducting polymers (ionomers) have emerged as essential materials for electrochemical CO_2 reduction reaction (CO_2RR) for sustainable chemical production.[1−4] These materials enhance catalytic performance by anchoring catalysts, facilitating ion transport, and creating favorable local microenvironments at electrode surfaces.[5−8] In membrane electrode assembly (MEA) electrolyzers, the local reaction conditions and product distributions also depend strongly on the membrane type employed.[9−12] Anion-exchange membranes (AEMs) create alkaline environments that favor the formation of multicarbon (C_{2+}) products but permit the crossover of CO_2 as HCO_3^- and CO_3^{2-} along with anionic liquid products, which limits overall CO_2 utilization.[13,14] Cation-exchange membranes (CEMs) prevent this crossover and enable higher single-pass CO_2 conversion but often promote undesired hydrogen evolution reaction (HER) due to local acidification caused by rapid proton transport.[15−17] Recent efforts have explored CEM-based MEAs to produce CO with an improved selectivity. Various strategies have been implemented to overcome the low selectivity and poor stability caused by acidic conditions, including the incorporation of buffering ionomer layers to locally neutralize protons,[18,19] operation under elevated pressure to suppress diffusion of protons,[16] and introduction of alkali cations (e.g., Cs^+) to modulate interfacial distribution of cations.[15] These approaches aim to establish alkaline microenvironments near the catalysts, thereby suppressing the HER and promoting selective CO_2RR. Advancing the performance of MEA further depends on developing ionomers that preserve these alkaline microenvironments under acidic bulk conditions, which can reduce side reactions and enhance operational stability. Ionomers applied to gas diffusion electrodes (GDEs) significantly improve the mass transport of CO_2 and enable stable operation at current densities exceeding hundreds of mA cm^{-2}.[20] Nevertheless, systematic studies specifically focusing on tailored ionomers to optimize CEM-based electrolyzers remain limited and are essential to fully exploiting their advantages for efficient CO_2RR.

Recent strategies for enhancing ionomer performance include optimizing their distribution within catalyst layers, tailoring ionomer−catalyst interactions, and controlling the microenvironment near the electrode surface.[21−25] Hydro-

Received: May 26, 2025
Revised: June 22, 2025
Accepted: July 2, 2025

https://doi.org/10.1021/acscatal.5c03583
ACS Catal. 2025, 15, 12222−12230

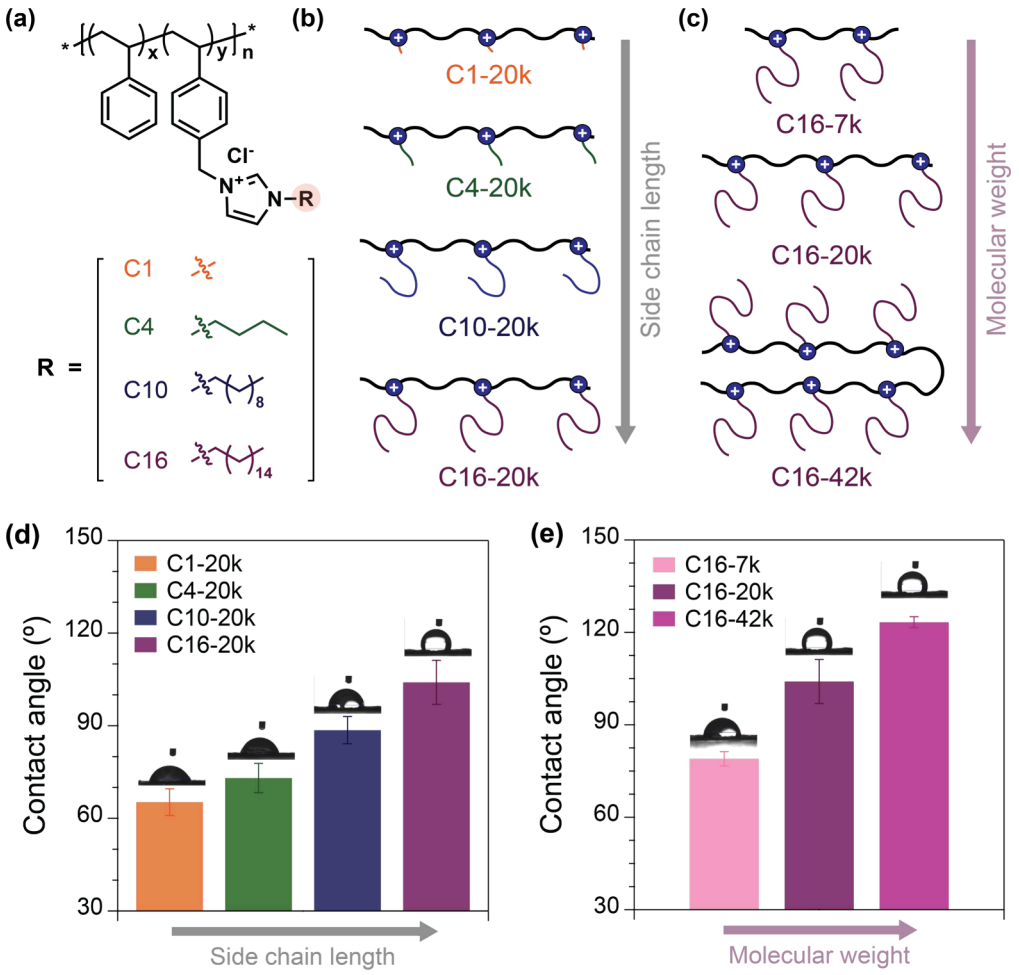

Figure 1. (a) Chemical structures of 1-*n*-alkylimidazolium ionomers with *n*-alkyl side chains of varying lengths: methyl (C1), *n*-butyl (C4), *n*-decyl (C10), and *n*-hexadecyl (C16). (b and c) Schematic illustrations of ionomers with systematic variations in (b) side chain length (C1-, C4-, C10-, and C16-20k) at a fixed molecular weight of 20 kg mol^{-1} and (c) molecular weight (C16-7k, C16-20k, and C16-42k) at a fixed alkyl side chain length of C16. Each set of ionomers was employed to examine the effects of side chain length and molecular weight on CO_2RR activity and selectivity. (d and e) Water contact angles demonstrating increased hydrophobicity with (d) longer alkyl side chains and (e) higher molecular weights of the ionomers.

phobic ionomers can notably alter electrolyte distribution, electrode wetting behavior, and local CO_2 concentration near catalyst sites.[26] Modification of polymer side chains or ionic head groups also impacts ion transport properties, interfacial pH buffering, and ionomer interactions with catalysts, thereby directly influencing reaction kinetics and product selectivity.[24,27,28] Such influences are especially pronounced in systems where the CO selectivity is highly sensitive to the interfacial pH and the transport of CO_2. While commercial ionomers such as Nafion, Sustainion, and PiperION have been widely studied with Ag-based catalysts, substantial structural differences among them complicate direct comparisons and hinder the establishment of generalized design principles.[29,30] To overcome these limitations, we adopted a systematic approach by isolating the effect of alkyl side chain length, varying only this parameter while maintaining a consistent polymer backbone and ionic head group. This controlled comparison provides clear structure−performance relationships, clarifying complexities associated with multicomponent ionomer systems and guiding the rational design of advanced ionomers tailored for CEM-based CO_2 electrolysis.

This work presents the design and synthesis of a series of 1-*n*-alkylimidazolium ionomers with varying alkyl side chain lengths (C_nH_{2n+1} where n = 1, 4, 10, and 16) while maintaining a common styrene-based polymer backbone and a fixed imidazolium ion-conducting group. CO_2RR experiments using Ag catalysts in a two-compartment cell (H-cell) revealed that longer side chains enhance CO_2RR selectivity, with the *n*-hexadecyl (n = 16) variant achieving the highest Faradaic efficiency (FE) for the CO_2RR of 90.1% and a corresponding FE_{H_2} of 3.6%. Notably, this ionomer also exhibited unusually high selectivity toward $HCOO^-$ of up to 17.9% at more negative potentials, suggesting an elevated interfacial pH at the catalyst−ionomer interface. Motivated by this unexpected behavior, we further investigated the *n*-hexadecyl ionomer in a CEM-based MEA configuration, where membrane-induced acidic microenvironments favor HER but could be offset by local alkalinity from the ionomer. Implementing a GDE within the MEA enhanced CO_2 transport and ensured proton availability from the acidic membrane environment, inherently suppressing reaction pathways toward $HCOO^-$ and enabling selective production of CO. The performance of the *n*-hexadecyl ionomer surpassed both commercial Sustainion XA-9 and its methyl-substituted analog (n = 1) in terms of FE_{CO} and partial current density for CO. To elucidate the underlying

https://doi.org/10.1021/acscatal.5c03583
ACS Catal. 2025, 15, 12222−12230

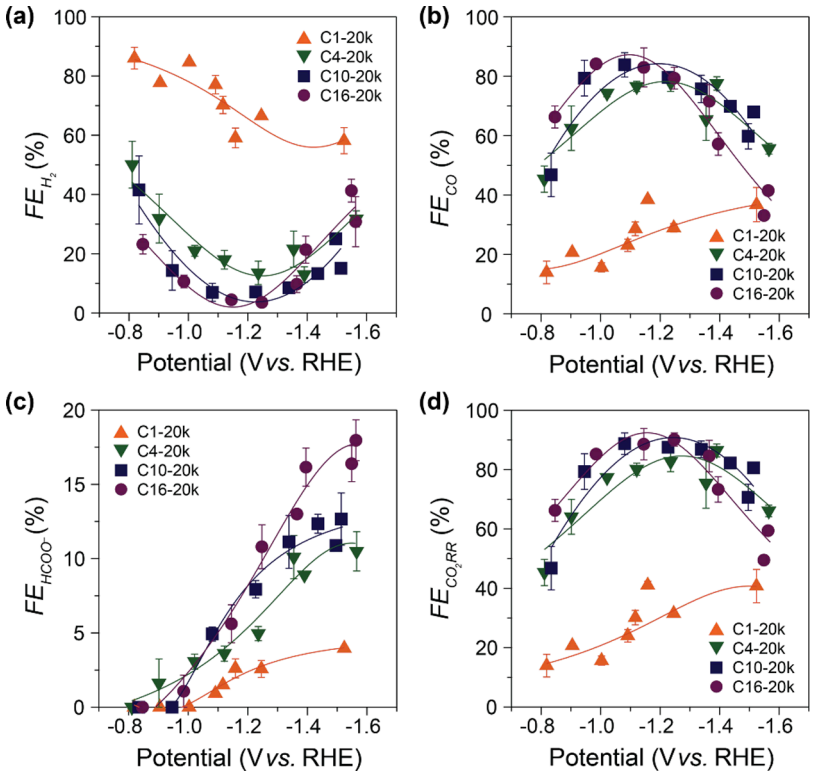

Figure 2. (a) FE_{H_2}, (b) FE_{CO}, (c) FE_{HCOO^-}, and (d) FE_{CO_2RR} on Ag-based electrodes coated with 1-*n*-alkylimidazolium ionomers: C1-20k (orange, triangle), C4-20k (green, inverted triangle), C10-20k (blue, square), and C16-20k (purple, circle). Experiments were conducted in an H-cell using a CO_2-saturated 0.1 M $KHCO_3$ electrolyte from −0.8 to −1.6 V. Error bars represent the standard deviation from at least three measurements. Lines connecting data points represent fitted curves serving as visual guides to potential-dependent trends.

mechanisms driving these performance improvements, additional experiments were conducted by systematically varying electrolyte concentration and bulk pH. These experiments confirmed that bulk electrolyte conditions could not account for the observed behavior, supporting the conclusion that the side chain structure plays a dominant role in shaping interfacial microenvironments. Collectively, these results establish a clear structure−performance relationship and offer molecular-level design principles for ionomers engineered for efficient and selective CO_2 electrolysis.

2. RESULTS AND DISCUSSION

A series of 1-*n*-alkylimidazolium ionomers with systematically varied *n*-alkyl side chain lengths and molecular weights was synthesized using a modified literature procedure.[23] The polystyrene backbone was chosen for its synthetic simplicity, negligible ionic conductivity, and polymerization compatibility, providing a suitable platform to isolate the effects of side chains and molecular weights. Three parent copolymers, poly(styrene-*co*-4-vinylbenzyl chloride) (P(S-*co*-VBC)), were synthesized by reversible addition−fragmentation chain transfer (RAFT) polymerization to yield controlled molecular weights of 7, 20, and 42 kg mol^{-1} with dispersity values between 1.16 and 1.41 (Table S1). The 20 kg mol^{-1} copolymer was functionalized with 1-*n*-alkylimidazoles containing linear alkyl side chains of different lengths (methyl, *n*-butyl, *n*-decyl, and *n*-hexadecyl) to produce four distinct ionomers (Figure 1a,b). Additional ionomers were obtained by grafting 1-*n*-hexadecylimidazole onto the 7 and 42 kg mol^{-1} copolymers (Figure 1c). These ionomers are denoted as C*x*-M_n, where *x* indicates the number of carbon atoms in the linear alkyl side chain and M_n denotes the number-average molecular weight of the parent copolymer. These synthesized ionomers are categorized into two sets for clarity: one set varying side chain lengths (Figure 1b: C1-20k, C4-20k, C10-20k, and C16-20k) and another set varying molecular weights at a fixed side chain length of C16 (Figure 1c: C16-7k, C16-20k, and C16-42k). Full synthetic details and characterization data, including ^{1}H NMR spectra, ion-exchange capacity (IEC), ionic conductivity (σ), gel permeation chromatography traces, and thermal stability profiles, are provided in the Supporting Information (Experimental, Figures S1−S3, and Tables S1−S4).

IEC and ionic conductivity were measured to assess ion transport properties as functions of the alkyl side chain length and molecular weight. IEC decreases with increasing alkyl side chain length due to the dilution of ionic groups, accompanied by corresponding reductions in ionic conductivity (Table S2). The nearly constant σ/IEC ratio indicates that conductivity losses arise mainly from lower ionic content rather than diminished ion mobility.[23] For ionomers with a fixed C16 side chain, IEC remains constant across molecular weights, while conductivity peaks at 20 kg mol^{-1} (Table S3). This trend reflects an optimal balance between ion dissociation and polymer segmental mobility.[31,32] Conductivity declines at 7 kg mol^{-1} owing to limited phase separation that likely restricts ion transport pathways, whereas at 42 kg mol^{-1} it drops again as chain entanglement and steric hindrance impede segmental motion.

Each ionomer was then integrated into Ag-based GDEs to examine how their structures translate to practical catalytic environments. Electrodes were fabricated by spray-coating

https://doi.org/10.1021/acscatal.5c03583
ACS Catal. 2025, 15, 12222−12230

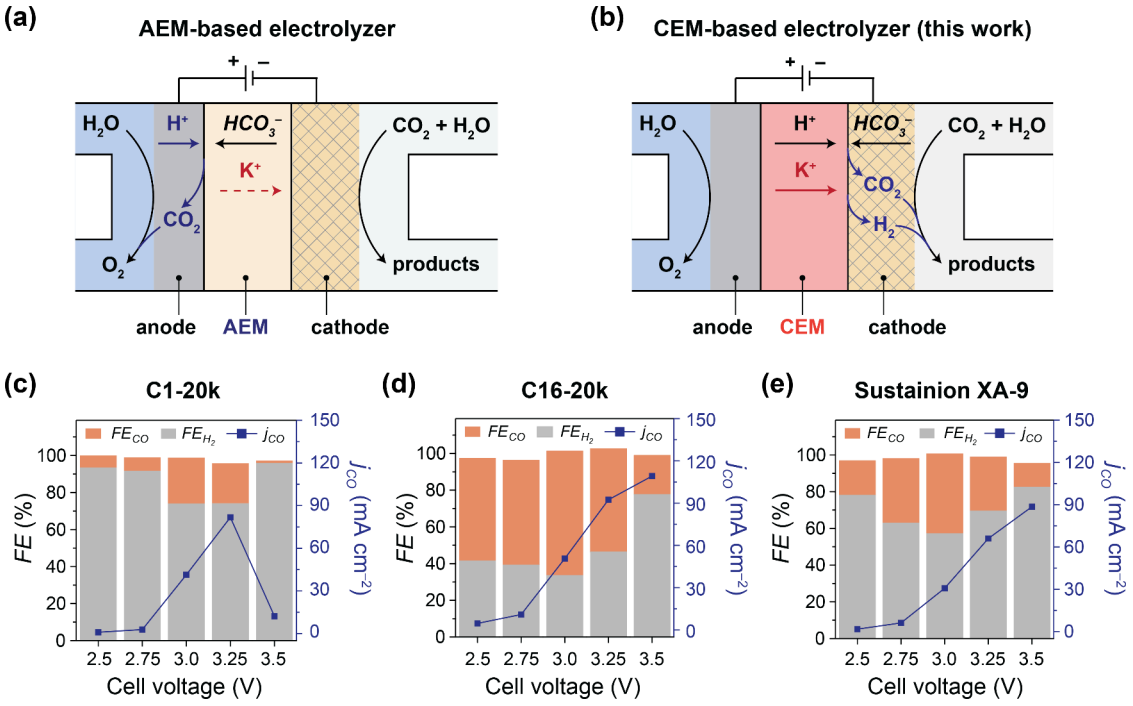

Figure 3. (a and b) Comparison of MEA architectures based on (a) AEMs and (b) CEMs. AEMs create alkaline microenvironments favorable for the CO_2RR but allow crossover of CO_2. CEMs enable higher single-pass CO_2 conversion but often promote undesired hydrogen evolution. (c–e) FE_{CO} and FE_{H_2} (left *y*-axis) and j_{CO} (right *y*-axis) for Ag-based electrodes coated with different ionomers in an MEA electrolyzer using a Nafion 211 membrane: (c) C1-20k, (d) C16-20k, and (e) Sustainion XA-9 ionomer. Measurements were conducted at cell voltages from 2.5 to 3.5 V using 0.1 M $KHCO_3$ as an anolyte.

commercial Ag nanoparticles (NPs, 20–40 nm) mixed with ionomers onto a gas diffusion layer (GDL). X-ray diffraction (XRD) and transmission electron microscopy (TEM) confirmed the crystallinity of the Ag NPs (Figure S4). Scanning electron microscopy and energy-dispersive X-ray spectroscopy (SEM/EDS) along with X-ray photoelectron spectroscopy (XPS) verified the uniform coverage of ionomers through the detection of nitrogen from the imidazolium groups (Figures S5 and S6). Water contact angle measurements demonstrate that hydrophobicity increases with longer side chains and higher molecular weights (Figure 1d,e). Contact angles rise progressively from 65° for C1-20k to 104° for C16-20k and reach 123° for C16-42k. Water uptake and swelling ratio were also measured for ionomers from C1-20k to C10-20k to further validate the trends in hydrophobicity with increasing alkyl side chain length. Both properties consistently decreased with longer side chains, confirming reduced accessibility to water and enhanced interfacial hydrophobicity (Table S4). These characterization results establish that the synthesized ionomers retain NP integrity, fully coat the catalyst surface, and systematically modulate the electrode wettability for subsequent CO_2RR studies.

CO_2RR experiments were performed using as-prepared electrodes in an H-cell containing a CO_2-saturated 0.1 M $KHCO_3$: four that vary side chain length at 20 kg mol^{-1} (Figure 1b) and three that vary molecular weight at a fixed side chain length of C16 (Figure 1c). FE and partial current densities (*j*) for CO, H_2, $HCOO^-$, and total CO_2RR products were collected as a function of applied potential (Figure 2; Figures S7–S10). All potentials are reported with respect to the reversible hydrogen electrode (RHE). Complete fabrication details and data analysis protocols are provided in the Supporting Information. The potential-dependent trends observed in FE clearly illustrate the impact of the side chain length in ionomers on their performance. FE_{H_2} initially decreases as potentials become more negative, reaching a minimum at approximately −1.2 V before slightly increasing at more negative potentials (Figure 2a). Conversely, FE_{CO} shows a peak between −1.0 and −1.2 V, after which it declines at more negative potentials due to the dominance of the HER and limitations in mass transport of aqueous CO_2 (Figure 2b). Ionomers with longer side chains strongly suppress HER while enhancing the CO_2RR. At −1.24 V, C1-20k exhibits an FE_{H_2} of 66.5% and an FE_{CO} of 28.9%, while C16-20k reduces FE_{H_2} to 3.6% and raises FE_{CO} to 79.3%. Notably, the production of $HCOO^-$ steadily increases as potentials become more negative, reaching a maximum FE of 17.9% with C16-20k at −1.56 V (Figure 2c). Although Ag typically favors CO production, previous studies have shown that $HCOO^-$ can become a major product under strongly alkaline bulk conditions (pH > 12).[33,34] In contrast, significant $HCOO^-$ production was observed in these experiments despite using a neutral, CO_2-saturated 0.1 M $KHCO_3$ bulk electrolyte. This result may indicate the formation of highly alkaline interfacial microenvironments with hydrophobic ionomers, particularly those with longer alkyl side chains, which suppress HER and enhance the CO_2RR. This interpretation aligns with conductivity data (Table S2) where reduced ionic conductivity from longer side chains likely limits OH^- mobility and elevates interfacial pH.

Tuning the molecular weight at the optimal side chain length of C16, which likely most effectively promotes local alkaline conditions, shows similar trends. C16-20k exhibits the strongest suppression of HER, the highest FE_{CO}, and the

https://doi.org/10.1021/acscatal.5c03583
ACS Catal. 2025, 15, 12222−12230

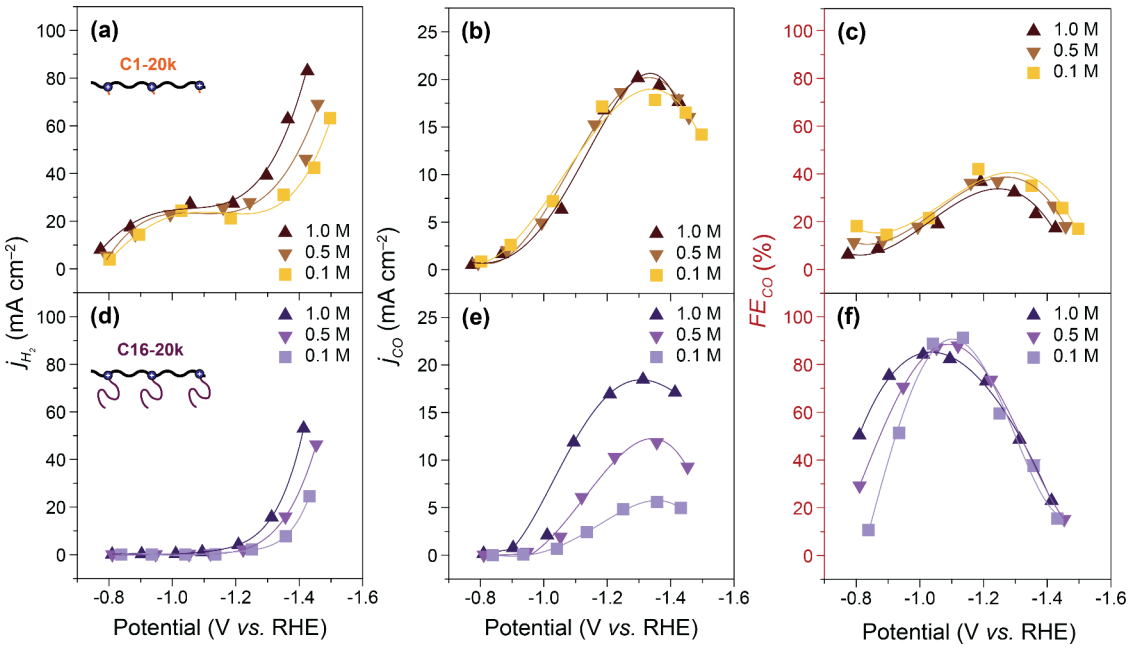

Figure 4. (a and d) j_{H_2}, (b and e) j_{CO}, and (c and f) FE_{CO} on Ag-based electrodes coated with 1-*n*-alkylimidazolium ionomers. The measurements were conducted in H-cells with varying HCO_3^- concentrations and a fixed K^+ concentration of 1.0 M. (a–c) C1-20k and (d and f) C16-20k ionomers evaluated in 1.0 M (triangle), 0.5 M (inverted triangle), and 0.1 M (square) HCO_3^- electrolytes. Insets depict the molecular structures of the respective ionomers.

highest FE_{HCOO^-} (Figure S9), consistent with optimal ionic conductivity at the intermediate molecular weight of 20 kg mol^{-1} (Table S3). These results indicate that the intermediate molecular weight across our samples provides an optimal microenvironment for selectivity independent of the intermediate hydrophobicity. This observation suggests that structural factors governed by molecular weight rather than hydrophobicity predominantly determine the reaction outcome. These structural effects were further evaluated using Sn catalysts (Figures S11–S13), which primarily produce $HCOO^-$, to verify whether side chain effects extend to other catalyst systems. At −1.45 V, the C16-20k electrode delivers an FE_{HCOO^-} of 84.6% and an FE_{H_2} of 9.6%, outperforming the C1-20k, which yields 64.3% and 26.5%, respectively (Figure S14). In terms of partial current densities, j_{HCOO^-} is similar between C1-20k and C16-20k, while C16-20k exhibits lower j_{H_2} and j_{CO} values (Figure S15). These results align with a previous report on Sn catalysts demonstrating enhanced selectivity for $HCOO^-$ on a hydrophobic surface of the electrode.[35] This trend mirrors the behavior observed in the Ag-based system and confirms that increased hydrophobicity suppresses the HER while maintaining or enhancing the CO_2RR across different catalyst systems. The consistent selectivity response across both metals highlights the general applicability of side chain engineering in tailoring electrode microenvironments for efficient and selective CO_2 electrolysis. Following this initial evaluation of the ionomers in the H-cell, an MEA was employed to demonstrate their performance under industrially relevant operating conditions. Subsequently, further characterizations in the H-cell were performed to elucidate the mechanistic details observed in an MEA by leveraging the simpler experimental design to obtain clear insights.

The performance of C16-20k at high current densities was further evaluated in CEM-based MEA systems in which maintaining local alkaline environments remains challenging (Figure 3b). Again, CEMs limit CO_2 crossover but impose acidic conditions that often favor HER. Hydrophobic, anion-exchange ionomers with restricted proton permeability offer a route to stabilize local alkalinity at the cathode and suppress HER.[20] To test this hypothesis, C1-20k and C16-20k were integrated into Ag-based GDEs within MEAs using Nafion 211 membranes, with a commercial Sustainion XA-9 ionomer included as a benchmark. All MEA tests employed a 0.1 M $KHCO_3$ anolyte and followed the electrode preparation protocol established for H-cell studies. C16-20k achieves the highest FE_{CO} of 68.7%, surpassing Sustainion (44.0%) and C1-20k (24.7%) at 3.0 V (Figures 3c–e and S16). j_{CO} increases with voltage, reaching 109.2 mA cm^{-2} for C16-20k at 3.5 V, while C1-20k remains limited at 12.2 mA cm^{-2}, reflecting dominant HER. The abrupt collapse of j_{CO} for C1-20k at 3.5 V is likely due to precipitation of salts and flooding caused by the crossover of K^+ ions through the CEM, hindering mass transport of CO_2 and accelerating HER.[36] Consequently, C1-20k exhibits the highest total current density of 965.8 mA cm^{-2} at 3.5 V, predominantly driven by the HER (Figure S17). In contrast, C16-20k suppresses the HER more effectively and thus lowers its total current density to 498.4 mA cm^{-2} at the same voltage. It is important to note that $HCOO^-$ production remained negligible across all voltages, indicating a distinct reaction environment in the MEA setup. Compared with the aqueous H-cell system, the CEM-based, gas-fed MEA configuration enhances CO_2 transport and ensures sufficient proton availability from the acidic membrane environment, inherently suppressing pathways toward $HCOO^-$ production and selectively promoting CO formation. Similar trends were observed in AEM-based systems where C16-20k also exhibited superior performance with significantly enhanced FE_{CO} and reduced operating voltages compared to C1-20k (Figures 3a and S18). These results highlight the practical advantages of hydrophobic ionomer design for improving CEM-based MEA

https://doi.org/10.1021/acscatal.5c03583
ACS Catal. 2025, 15, 12222−12230

performance and set the stage for mechanistic analysis of how the alkyl side chain length modulates interfacial alkaline microenvironments.

To understand the mechanistic origin of enhanced CO_2RR performance with long alkyl side chains, we evaluated how the ionomer structure governs interfacial microenvironments in H-cells under two distinct electrolyte conditions: lean electrolyte and acidic media. Lean electrolyte operation is desirable in MEAs to minimize salt precipitation from K^+ accumulation and prevent electrode flooding that limits long-term stability.[19] Acidic conditions, on the other hand, arise in CEM-based configurations due to rapid proton transport and tend to favor the HER. Understanding ionomer behavior under each of these constraints is essential for designing robust systems that sustain microenvironments for stable and selective operation. Electrolytes were thus designed to decouple the effects of bulk composition by varying (1) HCO_3^- concentration and (2) pH, with the fixed concentrations of K^+ of 1.0 and 0.1 M, respectively, to eliminate cation-dependent effects on CO_2RR (see Supporting Information).[37] These studies aimed to identify how the molecular structure of ionomers influences reaction selectivity across practical operating conditions relevant to CEM-based MEA devices.

We first investigated how changes in proton donor availability affect the reaction microenvironment using 1.0, 0.5, and 0.1 M HCO_3^- electrolytes. For C1-20k, j_{H_2} increases with HCO_3^- concentration at low overpotentials, plateaus near −1.1 V due to the depletion of HCO_3^-, and rises again at more negative potentials where H_2O serves as the dominant proton source (Figure 4a).[27] Meanwhile, j_{CO} remains relatively constant across concentrations, consistent with the previous report suggesting that CO_2 adsorption limits CO formation rather than the proton supply (Figure 4b). This behavior reflects a less hydrophobic interface that allows for sufficient access to both H_2O and HCO_3^- as proton donors. As a result, the selectivity for H_2 declines, and that for CO consistently improves with decreasing HCO_3^- concentration (Figures S19a and 4c).

C16-20k displays contrasting behavior. The higher hydrophobicity reduces interfacial water content and thus limits proton availability from both HCO_3^- and H_2O. This restriction in proton access enhances local alkalinity and creates microenvironments highly favorable for selective CO_2RR. Consequently, across all potentials, j_{CO} decreases markedly with decreasing HCO_3^- concentration (Figure 4e), while j_{H_2} decreases only at potentials more negative than −1.1 V (Figure 4d). Despite this reduction in j_{CO}, FE_{CO} remains stable at high overpotentials (Figure 4f), indicating that the HER is also suppressed to a similar extent. At lower overpotentials, however, CO production depends more heavily on protons from HCO_3^-, explaining the observed decline in FE_{CO} at lower bulk HCO_3^- concentrations. These observations suggest that C16-20k restricts H_2O access and therefore makes HCO_3^- its primary proton source, even under highly negative potentials.[25,38] These results confirm that the hydrophobic interface of C16-20k imposes kinetic restrictions on proton transport yet supports selective CO_2RR under lean electrolyte conditions, suppressing HER while sustaining CO selectivity at elevated overpotentials. This behavior underscores the potential of hydrophobic ionomers to achieve high selectivity for the CO_2RR in dilute electrolytes or even pure water systems. The stable CO production and suppressed HER under conditions of limited proton availability further emphasize the critical role of effective proton exclusion at the interface for maintaining selectivity in MEA operations.

Subsequently, the influence of the bulk pH was assessed using neutral (pH 6.8) and acidic (pH 3.1) electrolytes. In acidic media, C1-20k exhibits consistently higher FE_{H_2} and lower FE_{CO} across all potentials (Figure 5a,c), accompanied by

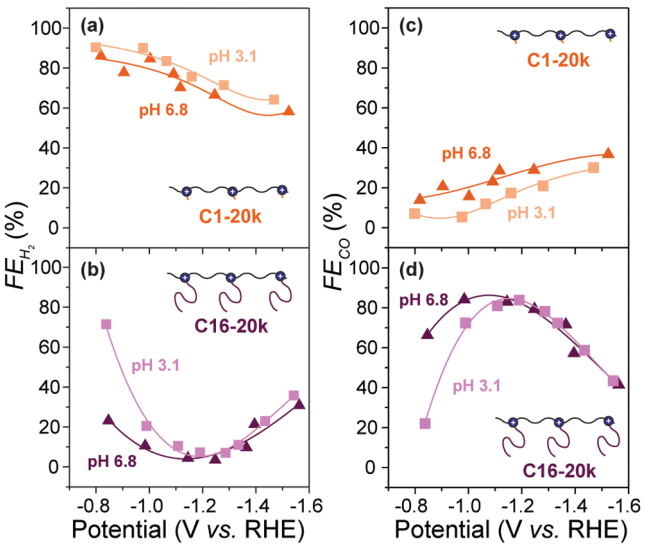

Figure 5. FE_{H_2} and FE_{CO} on Ag-based electrodes coated with 1-*n*-alkylimidazolium ionomers measured in H-cells under different pH conditions with a fixed K^+ concentration of 0.1 M. (a and c) C1-20k and (b and d) C16-20k were evaluated in electrolytes under neutral (pH 6.8) and acidic (pH 3.1) conditions. Insets depict the molecular structures of the respective ionomers.

a decrease in j_{CO} and little change in j_{H_2} (Figure S24a,b). These results imply that protons in the acidic bulk electrolyte readily permeate the less hydrophobic interface, lowering the interfacial pH and suppressing the CO_2RR. This susceptibility of C1-20k highlights the critical need for interfacial control under varying electrolyte pH. In contrast, C16-20k maintains stable selectivity even in acidic electrolytes. Below −1.2 V, both FE_{CO} and FE_{H_2} remain similar between neutral and acidic conditions (Figure 5b,d). Although the onset of $HCOO^-$ formation is slightly delayed (from −1.0 V under neutral conditions to −1.3 V in acid, Figure S23c), the similarly high FE_{HCOO^-} at high overpotentials indicates that an alkaline microenvironment is preserved at the catalyst interface despite acidic bulk conditions. This behavior likely arises from restricted OH^- diffusion into the bulk electrolyte,[39] which decouples interfacial pH from the surrounding electrolyte. The convergence of partial current densities for each product across pH conditions further supports this interpretation (Figure S25).

These systematic investigations under controlled conditions of bulk electrolytes indicate that the structure of ionomers plays a dominant role in modulating the interfacial microenvironment and thereby governs the performance of CO_2RR. Even under fixed concentrations of K^+, the performance trends of CO_2RR varied with the ionomer, indicating that the local distribution and hydration of cations are regulated by ionomer-specific interactions.[40] This interpretation emphasizes that the interfacial microenvironment is largely governed by the

https://doi.org/10.1021/acscatal.5c03583
ACS Catal. 2025, 15, 12222−12230

ionomer through its influence on the local behavior of the cations. Control experiments were further conducted using a CEM-based MEA fed with pure water to validate this hypothesis (Figure S26). Without K^+, formation of the electric double layer (EDL) was suppressed, limiting the establishment of a favorable interfacial microenvironment for the CO_2RR. Despite a significant reduction, selectivity toward CO remained measurable and was higher for C16-20k compared to C1-20k. Specifically, C16-20k exhibited a maximum FE_{CO} of 15.2% at 3.0 V, whereas C1-20k reached only 6.8% at a higher cell voltage of 3.5 V. This reduced but measurable activity of C16-20k indicates that, even without K^+, its fixed charges and hydrophobic character can partially sustain a favorable interfacial microenvironment for CO production by enabling the formation of a weaker but intrinsic EDL. These findings underscore the importance of designing ionomers that effectively modulate interfacial microenvironments to optimize catalytic activity and selectivity across diverse operating conditions.

3. CONCLUSIONS

In summary, we systematically investigated how alkyl side chain length and molecular weight in 1-*n*-alkylimidazolium ionomers modulate interfacial microenvironments and control activity and selectivity in Ag-catalyzed CO_2RR. Electrochemical measurements in H-cells revealed that increasing alkyl side chain length significantly enhances selectivity for CO_2RR, with C16-20k achieving the highest FE_{CO_2RR} of 90.1% while reducing FE_{H_2} to 3.6%. For ionomers with a fixed side chain length of C16, optimal performance was achieved at a molecular weight of 20 kg mol^{-1}, balancing favorable segmental mobility and ionic conductivity. Further evaluation of C16-20k in CEM-based MEA systems demonstrated superior performance relative to both the relatively hydrophilic C1-20k and commercial Sustainion XA-9. Specifically, C16-20k exhibited an FE_{CO} of 68.7% at 3.0 V and a j_{CO} of 109.2 mA cm^{-2} at 3.5 V, a notable result given the intrinsic challenge of achieving high selectivity due to prevailing hydrogen evolution in membrane-induced acidic environments. These results underscore the advantages of hydrophobic ionomers in MEA applications, particularly under acidic conditions and scenarios with reduced electrolyte dependence. Controlled experiments varying electrolyte concentrations and pH clarified the origins of this robust performance. These studies confirmed that C16-20k sustains an alkaline microenvironment by limiting interfacial water availability and proton transport, effectively decoupling the interface from bulk electrolyte conditions. The versatility of these ionomers across different catalytic systems, including Ag-catalyzed CO production, Sn-catalyzed $HCOO^-$ generation, and previously reported Cu-catalyzed hydrocarbon synthesis,[23] highlights that optimal structures of ionomers strongly depend on the catalyst and system. This structural sensitivity underscores the need for continued systematic research to refine ionomer designs tailored to specific electrocatalytic applications. Investigations are currently underway to extend this strategy to diverse catalyst systems and device architectures, aiming to generalize design principles and advance the performance to an industrially relevant level.

■ ASSOCIATED CONTENT

Supporting Information

The Supporting Information is available free of charge at https://pubs.acs.org/doi/10.1021/acscatal.5c03583.

Experimental procedures, characterizations, Figures S1−S27, and Tables S1−S4(PDF)

■ AUTHOR INFORMATION

Corresponding Authors

Da Hye Won − *Clean Energy Research Center, Korea Institute of Science and Technology (KIST), Seoul 02792, Republic of Korea; Division of Energy & Environment Technology, KIST School, University of Science and Technology, Seoul 02792, Republic of Korea; KHU-KIST Department of Converging Science and Technology, Kyung Hee University, Seoul 02477, Republic of Korea;* orcid.org/0000-0002-7589-7866; Email: dahye0803@kist.re.kr

Jai Hyun Koh − *Clean Energy Research Center, Korea Institute of Science and Technology (KIST), Seoul 02792, Republic of Korea; Division of Energy & Environment Technology, KIST School, University of Science and Technology, Seoul 02792, Republic of Korea;* orcid.org/0000-0003-2589-8032; Email: jhkoh@kist.re.kr

Authors

Jihyun Park − *Clean Energy Research Center, Korea Institute of Science and Technology (KIST), Seoul 02792, Republic of Korea; Department of Chemical and Biological Engineering, Korea University, Seoul 02841, Republic of Korea*

Younghyun Chae − *Clean Energy Research Center, Korea Institute of Science and Technology (KIST), Seoul 02792, Republic of Korea; Division of Energy & Environment Technology, KIST School, University of Science and Technology, Seoul 02792, Republic of Korea*

Chanwoo Lee − *Clean Energy Research Center, Korea Institute of Science and Technology (KIST), Seoul 02792, Republic of Korea; Division of Energy & Environment Technology, KIST School, University of Science and Technology, Seoul 02792, Republic of Korea*

Gyeongjin Kwon − *Clean Energy Research Center, Korea Institute of Science and Technology (KIST), Seoul 02792, Republic of Korea*

Woong Hee Lee − *Clean Energy Research Center, Korea Institute of Science and Technology (KIST), Seoul 02792, Republic of Korea; Division of Energy & Environment Technology, KIST School, University of Science and Technology, Seoul 02792, Republic of Korea;* orcid.org/0000-0002-5779-3246

Hyo Sang Jeon − *Sustainable Energy Research Division, Korea Institute of Science and Technology (KIST), Seoul 02792, Republic of Korea;* orcid.org/0000-0003-3486-0589

Jinhan Cho − *Department of Chemical and Biological Engineering, Korea University, Seoul 02841, Republic of Korea;* orcid.org/0000-0002-7097-5968

Complete contact information is available at: https://pubs.acs.org/10.1021/acscatal.5c03583

Author Contributions

[⊥]J.P. and Y.C. contributed equally to this work.

Notes

The authors declare no competing financial interest.

■ ACKNOWLEDGMENTS

The authors are grateful for financial support from the institutional program grant from Korea Institute of Science and Technology (KIST); the National Research Council of Science & Technology (NST) grant (Grant No. CAP21011-100); and the "Carbon Upcycling Project for Platform Chemicals" of the National Research Foundation (Grant No. 2022M3J3A1050053), Korea.

■ REFERENCES

(1) Hori, Y. *Modern Aspects of Electrochemistry*; Springer: New York, NY, 2008; pp 89−189.
(2) Lee, W. H.; Kim, K.; Koh, J. H.; Lee, D. K.; Won, D. H.; Oh, H.-S.; Lee, U.; Min, B. K. The green-ol (green-alcohol) economy. *Nano Energy* **2023**, *110*, 108373.
(3) Chae, Y.; Kim, H.; Lee, D. K.; Lee, U.; Won, D. H. Exploring the critical role of binders in electrochemical CO_2 reduction reactions. *Nano Energy* **2024**, *130*, 110134.
(4) Zeng, F.; Deng, H.; Zhuansun, M.; Teng, W.; Wang, Y. Benchmarking ionomers for CO_2 electroreduction to multicarbon products in zero-gap electrolysers. *J. Mater. Chem. A* **2024**, *12*, 20990−20998.
(5) Higgins, D.; Hahn, C.; Xiang, C.; Jaramillo, T. F.; Weber, A. Z. Gas-diffusion electrodes for carbon dioxide reduction: A new paradigm. *ACS Energy Lett.* **2019**, *4*, 317−324.
(6) García de Arquer, F. P.; Dinh, C.-T.; Ozden, A.; Wicks, J.; McCallum, C.; Kirmani, A. R.; Nam, D.-H.; Gabardo, C.; Seifitokaldani, A.; Wang, X.; Li, Y. C.; Li, F.; Edwards, J.; Richter, L. J.; Thorpe, S. J.; Sinton, D.; Sargent, E. H. CO_2 electrolysis to multicarbon products at activities greater than 1 A cm^{-2}. *Science* **2020**, *367*, 661−666.
(7) Huang, J. E.; Li, F.; Ozden, A.; Sedighian Rasouli, A.; García de Arquer, F. P.; Liu, S.; Zhang, S.; Luo, M.; Wang, X.; Lum, Y.; Xu, Y.; Bertens, K.; Miao, R. K.; Dinh, C.-T.; Sinton, D.; Sargent, E. H. CO_2 electrolysis to multicarbon products in strong acid. *Science* **2021**, *372*, 1074−1078.
(8) Lu, X.; You, W.; Peltier, C. R.; Coates, G. W.; Abruña, H. D. Influence of ion-exchange capacity on the solubility, mechanical properties, and mass transport of anion-exchange ionomers for alkaline fuel cells. *ACS Appl. Energy Mater.* **2023**, *6*, 876−884.
(9) Ge, L.; Rabiee, H.; Li, M.; Subramanian, S.; Zheng, Y.; Lee, J. H.; Burdyny, T.; Wang, H. Electrochemical CO_2 reduction in membrane-electrode assemblies. *Chem.* **2022**, *8*, 663−692.
(10) Ozden, A.; García de Arquer, F. P.; Huang, J. E.; Wicks, J.; Sisler, J.; Miao, R. K.; O'Brien, C. P.; Lee, G.; Wang, X.; Ip, A. H.; Sargent, E. H.; Sinton, D. Carbon-efficient carbon dioxide electrolysers. *Nat. Sustain.* **2022**, *5*, 563−573.
(11) de Sousa, L.; Benes, N. E.; Mul, G. Evaluating the effects of membranes, cell designs, and flow configurations on the performance of Cu-GDEs in converting CO_2 to CO. *ACS ES&T Eng.* **2022**, *2*, 2034−2042.
(12) Habibzadeh, F.; Mardle, P.; Zhao, N.; Riley, H. D.; Salvatore, D. A.; Berlinguette, C. P.; Holdcroft, S.; Shi, Z. Ion exchange membranes in electrochemical CO_2 reduction processes. *Electrochem. Energy Rev.* **2023**, *6*, 1−35.
(13) Weng, L.-C.; Bell, A. T.; Weber, A. Z. Towards membrane-electrode assembly systems for CO_2 reduction: a modeling study. *Energy Environ. Sci.* **2019**, *12*, 1950−1968.
(14) Salvatore, D. A.; Gabardo, C. M.; Reyes, A.; O'Brien, C. P.; Holdcroft, S.; Pintauro, P.; Bahar, B.; Hickner, M.; Bae, C.; Sinton, D.; Sargent, E. H.; Berlinguette, C. P. Designing anion exchange membranes for CO_2 electrolysers. *Nat. Energy* **2021**, *6*, 339−348.
(15) Pan, B.; Fan, J.; Zhang, J.; Luo, Y.; Shen, C.; Wang, C.; Wang, Y.; Li, Y. Close to 90% single-pass conversion efficiency for CO_2 electroreduction in an acid-fed membrane electrode assembly. *ACS Energy Lett.* **2022**, *7*, 4224−4231.
(16) Park, J.; Kim, E.-D.; Kim, S.; Lim, C.; Kim, H.; Ko, Y.-J.; Choi, J.-Y.; Oh, H.-S.; Lee, W. H. Deriving an efficient and stable microenvironment for a CO_2 MEA electrolyzer by reverse osmosis. *ACS Energy Lett.* **2024**, *9*, 3342−3350.
(17) Delacourt, C.; Ridgway, P. L.; Kerr, J. B.; Newman, J. Design of an electrochemical cell making syngas ($CO+H_2$) from CO_2 and H_2O reduction at room temperature. *J. Electrochem. Soc.* **2008**, *155*, B42.
(18) Park, J.; Ko, Y.-J.; Lim, C.; Kim, H.; Min, B. K.; Lee, K.-Y.; Koh, J. H.; Oh, H.-S.; Lee, W. H. Strategies for CO_2 electroreduction in cation exchange membrane electrode assembly. *Chem. Eng. J.* **2023**, *453*, 139826.
(19) O'Brien, C. P.; Miao, R. K.; Liu, S.; Xu, Y.; Lee, G.; Robb, A.; Huang, J. E.; Xie, K.; Bertens, K.; Gabardo, C. M.; Edwards, J. P.; Dinh, C.-T.; Sargent, E. H.; Sinton, D. Single pass CO_2 conversion exceeding 85% in the electrosynthesis of multicarbon products via local CO_2 regeneration. *ACS Energy Lett.* **2021**, *6*, 2952−2959.
(20) Lees, E. W.; Mowbray, B. A. W.; Parlane, F. G. L.; Berlinguette, C. P. Gas diffusion electrodes and membranes for CO_2 reduction electrolysers. *Nat. Rev. Mater.* **2022**, *7*, 55−64.
(21) Mowbray, B. A. W.; Dvorak, D. J.; Taherimakhsousi, N.; Berlinguette, C. P. How catalyst dispersion solvents affect CO_2 electrolyzer gas diffusion electrodes. *Energy Fuels* **2021**, *35*, 19178−19184.
(22) Du, X.; Zhang, P.; Zhang, G.; Gao, H.; Zhang, L.; Zhang, M.; Wang, T.; Gong, J. Confinement of ionomer for electrocatalytic CO_2 reduction reaction via efficient mass transfer pathways. *Natl. Sci. Rev.* **2024**, *11*, nwad149.
(23) Song, Y. I.; Yoon, B.; Lee, C.; Kim, D.; Han, M. H.; Han, H.; Lee, W. H.; Won, D. H.; Kim, J. K.; Jeon, H. S.; Koh, J. H. Impact of side chains in 1-*n*-alkylimidazolium ionomers on Cu-catalyzed electrochemical CO_2 reduction. *Adv. Sci.* **2024**, *11*, e2406281.
(24) Jung, W.; Shin, S.-H.; Park, S.; Chae, Y.; Lee, U.; Cho, H. J.; Kim, S.; Hwang, Y. J.; Lee, J. Y.; Won, D. H. Unveiling key descriptors of ionomer materials for enhanced electrochemical CO_2 reduction. *ACS Energy Lett.* **2025**, *10*, 620−628.
(25) Park, S.; Kim, H.; Kim, D.; Chae, Y.; Baek, S.-W.; Lee, D. K.; Lee, U.; Won, D. H. Tuning the wettability of tandem electrodes affects CO_2 electro-conversion to multicarbon products. *Appl. Surf. Sci. Adv.* **2025**, *27*, 100727.
(26) Zhao, X.; Xie, H.; Deng, B.; Wang, L.; Li, Y.; Dong, F. Enhanced CO_2 reduction with hydrophobic cationic-ionomer layer-modified zero-gap MEA in acidic electrolyte. *Chem. Commun.* **2024**, *60*, 542−545.
(27) Koshy, D. M.; Akhade, S. A.; Shugar, A.; Abiose, K.; Shi, J.; Liang, S.; Oakdale, J. S.; Weitzner, S. E.; Varley, J. B.; Duoss, E. B.; Baker, S. E.; Hahn, C.; Bao, Z.; Jaramillo, T. F. Chemical modifications of Ag catalyst surfaces with imidazolium ionomers modulate H_2 evolution rates during electrochemical CO_2 reduction. *J. Am. Chem. Soc.* **2021**, *143*, 14712−14725.
(28) Xue, L.; Gao, Z.; Ning, T.; Li, W.; Li, J.; Yin, J.; Xiao, L.; Wang, G.; Zhuang, L. Dual-Role of Polyelectrolyte-Tethered Benzimidazolium Cation in Promoting CO_2/Pure Water Co-Electrolysis to Ethylene. *Angew. Chem., Int. Ed.* **2023**, *62*, No. e202309519.
(29) Liu, M.; Hu, H.; Kong, Y.; Montiel, I. Z.; Kolivoška, V.; Rudnev, A. V.; Hou, Y.; Erni, R.; Vesztergom, S.; Broekmann, P. The role of ionomers in the electrolyte management of zero-gap MEA-based CO_2 electrolysers: A Fumion vs. *Nafion comparison. Appl. Catal. B* **2023**, *335*, 122885.
(30) Chang, M.; Ren, W.; Ni, W.; Lee, S.; Hu, X. Ionomers modify the selectivity of Cu-catalyzed electrochemical CO_2 reduction. *ChemSusChem* **2023**, *16*, No. e202201687.
(31) Chae, J. E.; Yoo, S. J.; Kim, J. Y.; Jang, J. H.; Lee, S. Y.; Song, K. H.; Kim, H.-J. Hydrocarbon-based electrode ionomer for proton exchange membrane fuel cells. *Int. J. Hydrogen Energy* **2020**, *45*, 32856−32864.
(32) Zhou, J.; Joseph, K.; Ahlfield, J. M.; Park, D.-Y.; Kohl, P. A. Poly(arylene ether) ionomers with pendant quinuclidium groups and varying molecular weight for alkaline electrodes. *J. Electrochem. Soc.* **2013**, *160*, F573−F578.
(33) Gabardo, C. M.; Seifitokaldani, A.; Edwards, J. P.; Dinh, C.-T.; Burdyny, T.; Kibria, M. G.; O'Brien, C. P.; Sargent, E. H.; Sinton, D.

https://doi.org/10.1021/acscatal.5c03583
ACS Catal. 2025, 15, 12222−12230

Combined high alkalinity and pressurization enable efficient CO_2 electroreduction to CO. *Energy Environ. Sci.* **2018**, *11*, 2531−2539.
(34) Seifitokaldani, A.; Gabardo, C. M.; Burdyny, T.; Dinh, C.-T.; Edwards, J. P.; Kibria, M. G.; Bushuyev, O. S.; Kelley, S. O.; Sinton, D.; Sargent, E. H. Hydronium-induced switching between CO_2 electroreduction pathways. *J. Am. Chem. Soc.* **2018**, *140*, 3833−3837.
(35) Abarca, J. A.; Warmuth, L.; Rieder, A.; Dutta, A.; Vesztergom, S.; Broekmann, P.; Irabien, A.; Díaz-Sainz, G. GDE stability in CO_2 electroreduction to formate: The role of ionomer type and loading. *ACS Catal.* **2025**, *15*, 8753−8767.
(36) Li, M.; Idros, M. N.; Wu, Y.; Burdyny, T.; Garg, S.; Zhao, X. S.; Wang, G.; Rufford, T. E. The role of electrode wettability in electrochemical reduction of carbon dioxide. *J. Mater. Chem. A* **2021**, *9*, 19369−19409.
(37) Resasco, J.; Chen, L. D.; Clark, E.; Tsai, C.; Hahn, C.; Jaramillo, T. F.; Chan, K.; Bell, A. T. Promoter effects of alkali metal cations on the electrochemical reduction of carbon dioxide. *J. Am. Chem. Soc.* **2017**, *139*, 11277−11287.
(38) Lai, W.; Qiao, Y.; Wang, Y.; Huang, H. Stability issues in electrochemical CO_2 reduction: Recent advances in fundamental understanding and design strategies. *Adv. Mater.* **2023**, *35*, No. e2306288.
(39) Liang, H.-Q.; Zhao, S.; Hu, X.-M.; Ceccato, M.; Skrydstrup, T.; Daasbjerg, K. Hydrophobic copper interfaces boost electroreduction of carbon dioxide to ethylene in water. *ACS Catal.* **2021**, *11*, 958−966.
(40) Yang, X.; Ding, H.; Li, S.; Zheng, S.; Li, J.-F.; Pan, F. Cation-induced interfacial hydrophobic microenvironment promotes the C−C coupling in electrochemical CO_2 reduction. *J. Am. Chem. Soc.* **2024**, *146*, 5532−5542.

https://doi.org/10.1021/acscatal.5c03583
ACS Catal. 2025, 15, 12222−12230